Check for updates



www.chemcatchem.org

Mechanistic Investigation of an Organocatalytic Bromocyclization of O-Allyl Carbamates

Francisco Wanderson Moreira Ribeiro, [a] Jullyane Emi Matsushima, [b] Guilherme Obeid, [a] Elisângela Vinhato, [b] Alessandro Rodrigues, *[b] and Thiago Carita Correra*[a]

Intramolecular enantioselective halocyclization of olefins represents a valuable organic synthesis strategy. This work reports the enantioselective bromoaminocyclization of O-cinnamyl tosylcarbamate catalyzed by a Cinchona-derived organocatalyst as a model reaction to understand non-covalent catalyzed bromoaminocyclizations. The corresponding bromo-oxazinanone was obtained with excellent regio- and diastereoselectivity in 69% yield and 80:20 er, promoted by a thiocarbamatecinchonine catalyst. This reaction served as a compelling prototype for a comprehensive mechanistic investigation, combining experimental and theoretical approaches. Analysis of the reaction mixture by electrospray ionization mass spectrometry (ESI(+)-MS) and detailed evaluation of key intermediates via infrared multiphoton dissociation (IRMPD) spectroscopy were performed. The thermodynamic origins of enantioselectivity were explored by analyzing the potential energy surface of the reaction using density functional theory (DFT) calculations. This analysis included relevant transition states and intermediates, as well as the role of non-covalent interactions within the active catalytic species as revealed by natural bond orbital (NBO) analysis. Consistent with the experimental observations, DFT calculations indicated that the electrophilic bromo species is activated by the sulfur atom of the (thio)carbonyl group of the catalysts, and bromonium ion formation constitutes the enantiodetermining step, with a calculated overall reaction barrier of 27.0 kcal mol^{-1} .

1. Introduction

The halocyclization reaction of olefinic compounds, discovered over a century ago, evolved into a powerful tool for the synthesis of heterocycles.[1-3] Despite its importance, metalcatalyzed variants of halocyclization reactions only emerged in the literature several decades later, spurred by the pioneering works of Kitagawa and Taguchi.[4] Their contributions have significantly propelled the field of N- and Oheterocyclization reactions, encompassing halolactonization,^[5] haloetherification, [6,7] and haloaminocyclization. [8-15] These reactions enable the stereocontrolled formation of vicinal halocarbon and heteroatom-carbon bonds (Scheme 1)[16,17] leading to the evolution of catalytic systems capable of handling a broad range of substrates.^[2,18–33]

In this context, O-allyl carbamates have been proven to be effective substrates for the synthesis of valuable synthetic intermediates through metal-catalyzed transformations encompassing formal [3,3]-sigmatropic rearrangementsdecarboxylation,[34–38] decarboxylative C—H couplings,[39] aminoacetoxylations,^[40] aminohydroxylations,^[41] aminochlori nations, [42-47] and aminobrominations. [42,48-50] For instance, previous studies have reported the use of Fe(II), [45] Cu(II), [46] Pd(II),[42,43,47] and Sc(III)[48,50] as metal sources for catalyzed halocyclization reactions of O-allylic carbamates (Scheme 1a-g). As a complementary synthetic approach, Yang and coworkers developed the chloro-O-cyclization of O-allyl carbamates using a Cinchona-derived quaternary ammonium salt as a phase-transfer catalyst (PTC) (Scheme 1h).[51] These reactions lead to the regioselective cyclization of either 5-exo or 6-endo oxazolidinones and oxazinanones, which contain adjacent nitrogen and halogen (bromine or chlorine) groups.

Although metal-catalyzed strategies have been extensively explored for the haloaminocyclization reaction of O-allylic carbamates, no reports to date have described the development of an enantioselective organocatalytic approach for this transformation. This is particularly surprising considering the remarkable progress achieved in recent years utilizing organocatalysis for enantioselective halocyclization reactions with other substrates.^[28,33,52,53] Perhaps one of the reasons for the lack of organocatalyzed halocyclization variants, compared to the metal-based strategies, could be attributed to the absence of a generalized catalytic model to explain the organocatalysts' actions, especially for non-covalent organocatalysts, as

Francisco Wanderson Moreira Ribeiro and Jullyane Emi Matsushima contributed eaually to this work.

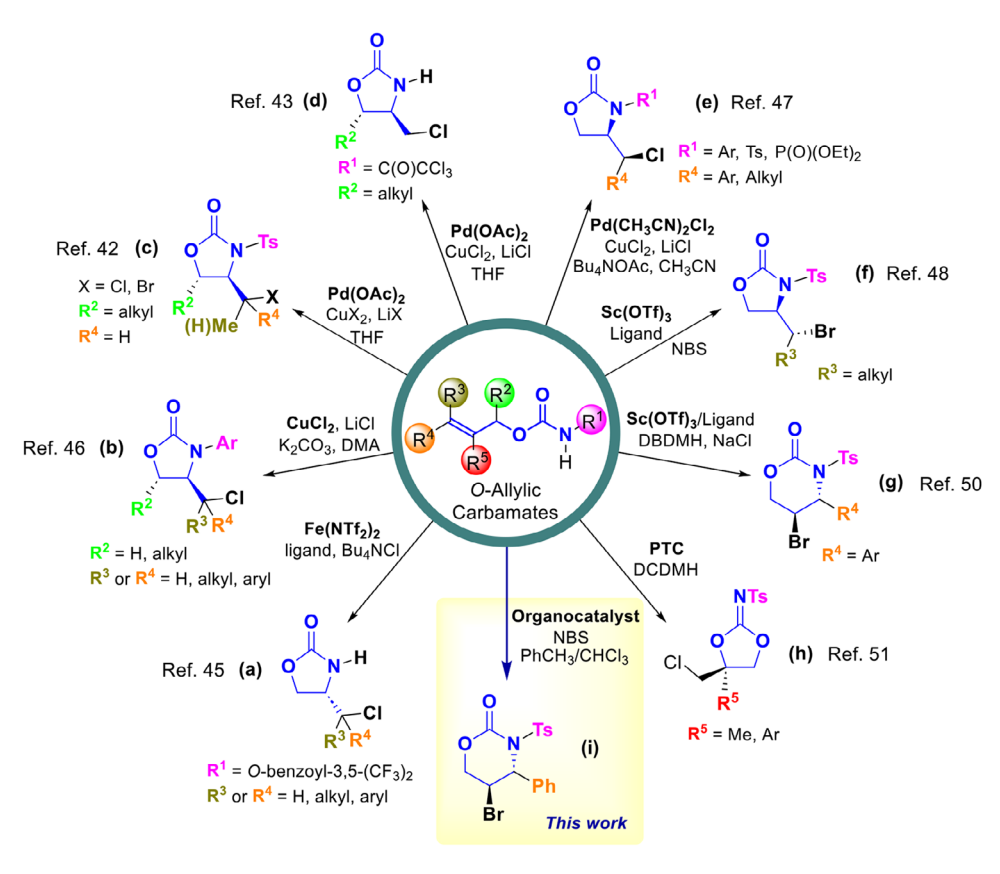
- Supporting information for this article is available on the WWW under https://doi.org/10.1002/cctc.202402004
- © 2025 The Author(s). ChemCatChem published by Wiley-VCH GmbH. This is an open access article under the terms of the Creative Commons Attribution License, which permits use, distribution and reproduction in any medium, provided the original work is properly cited.

[[]a] F. W. M. Ribeiro, G. Obeid, T. C. Correra Department of Fundamental Chemistry, Institute of Chemistry, University of Sao Paulo, Av. Prof. Lineu Prestes, 748, São Paulo 05508-000, Brazil E-mail: tcorrera@ig.usp.bi

[[]b] J. E. Matsushima, E. Vinhato, A. Rodrigues Departamento de Química, Universidade Federal de São Paulo, UNIFESP, Diadema, São Paulo 09972-270, Brazil E-mail: alessandro.rodrigues@unifesp.br

3, Downloaded from https://chemistry-europe.onlinelibrary.wiley.com/doi/10.1002/cctc.202402004 by Univ of Sao Paulo - Brazil, Wiley Online Library on [05/05/2025]. See the Terms and Conditions (https://onlinelibrary.wiley.com/terms

-and-conditions) on Wiley Online Library for rules of use; OA articles are governed by the applicable Creative Commons



Scheme 1. Examples (a-h) of vicinal halocarbon and hetero-carbon bond formation representing the context of (i) this work.

the characterization of the non-covalent interactions within the active catalytic structure is critical for understanding their activity.^[54–57]

Despite that, the field of organocatalysis has seen significant advancements since 2010, following the pioneering contributions of Borhan, [58] Fujioka, [59] Tang, [60] Yeung, [61] and their coworkers. Their work on cinchona alkaloid-catalyzed asymmetric intramolecular halocyclization of alkenes and alkynes established organocatalysis as a key methodology for these transformations. Since then, numerous functionalized molecules have been synthesized through asymmetric halocyclization reactions employing cinchona alkaloid-derived organocatalysts. In this context, cinchona-based organocatalysts are considered a relevant model system for non-covalent organocatalysts. Building on previous reports in this area, two major pathways were proposed to hypothesize the bromocyclization mechanism for carbamate 1, as shown in Scheme 2.

Considering Cheng and coworkers report in similar transformations, [62] these reactions may start with the halogen transfer to the organocatalyst thiocarbamate nitrogen or sulfur atoms, forming two different isomeric intermediate AI and AII (Scheme 2). Species AIII (Scheme 2) was also considered as a possible intermediate based on an analog of intermediate proposed by Whitehead and coworkers that suggested a chlorolactonization reaction to proceed via a halogen transfer to quinuclidinic nitrogen of the catalyst. [63] Despite the halogen insertion site, intermediate A would bind with the substrate 1 to produce a halonium intermediate, [64] leading to the formation

of product ${\bf 2}$ and subsequent organocatalyst regeneration after additional reaction steps.

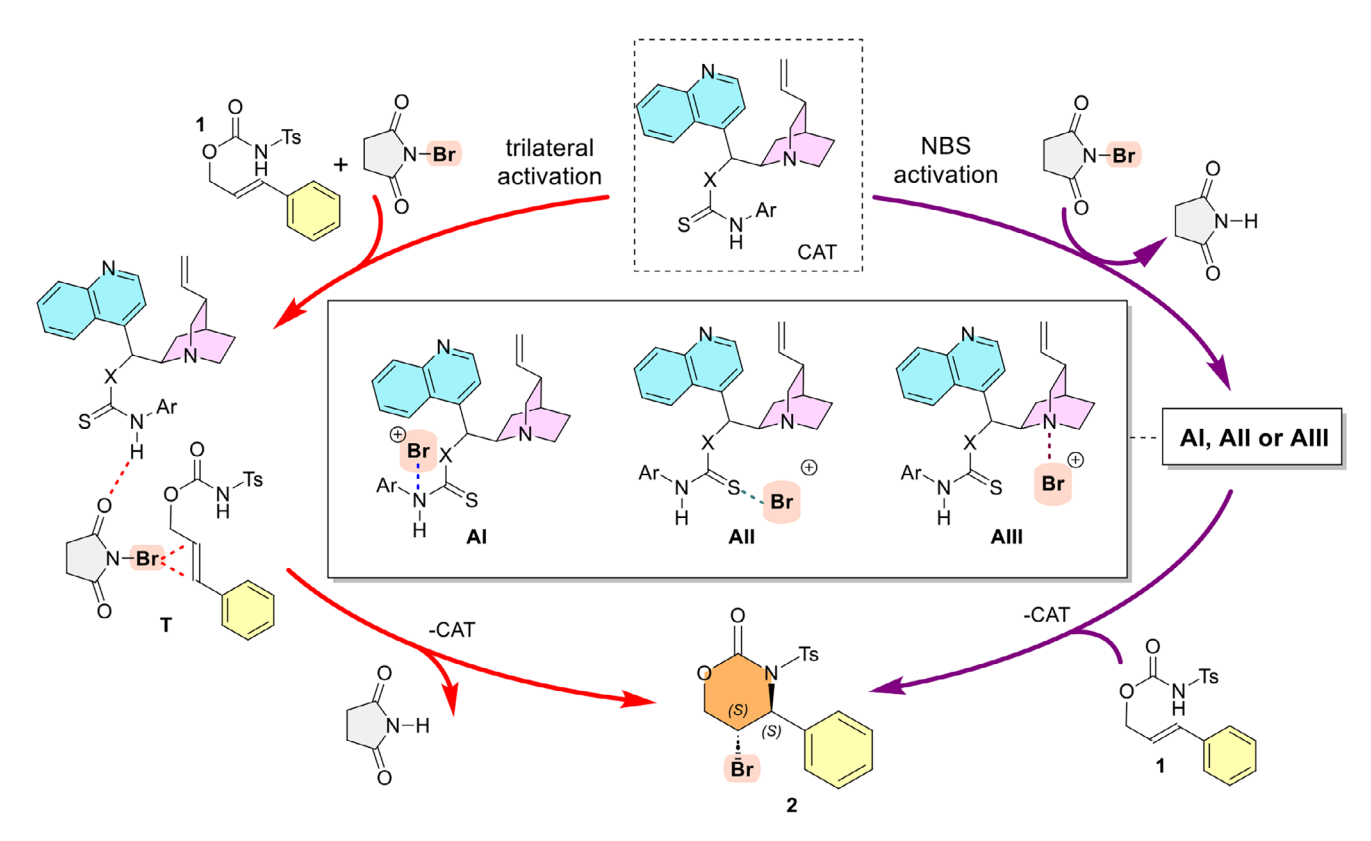
Zhang and coworkers $^{[65]}$ evaluated the bromolactonization of (Z)-1,3-enynes and suggested the formation of a net of hydrogen bonds involving the halogen source (NBS), the organocatalyst, and the substrate. Based on this proposal, a trilateral complex T (Scheme 2) was also considered a possible reaction pathway for the title reaction.

In light of these factors and based on Yeung and coworkers reports for organocatalytic electrophilic bromolactonization and bromolactamization reactions, [17,61,62,66-69] we envision that *Cinchona* alkaloid derivatives could be used as an enantioselective model for non-covalent catalysis to the bromoaminocyclization of *O*-cinnamyl carbamate 1. Therefore, we present an experimental and theoretical mechanistic study of the catalytic abilities of selected *Cinchona* alkaloid derivatives as organocatalysts for the enantioselective bromoaminocyclization of *O*-cinnamyl carbamate 1 (Scheme 1i) as a model reaction for non-covalent catalyzed bromoaminocyclizations.

Considering the propositions presented in Scheme 2, three major points will be evaluated: (i) the presence of trilateral and NBS activation pathways, (ii) the Br insertion site as part of the NBS activation pathway, and (iii) the structure and non-covalent network of the relevant species involved in the reaction.

To that end, the synthesis and evaluation of *Cinchona*-derived organocatalysts and the optimization of reaction conditions were carried out followed by a comprehensive mechanistic study, which was developed by combining ESI(+)-MS,

8. Dowloaded from https://teneintry-europe.onlinelbtrary.wiely.com/doi/10.1002/ccc.2.02402004 by Univ of Sao Paulo - Brazil, Wiley Online Library on [05.052025]. See the Terms and Conditions (https://onlinelibrary.wiely.com/terms-and-conditions) on Wiley Online Library for rules of use; OA articles are governed by the applicable Creative Commons



Scheme 2. Possible pathways considered in this work for *O*-allyl carbamate 1 bromoaminocyclization mediated by NBS and catalyzed by a *Cinchona*-based organocatalyst, inspired by previous reports on similar transformations (see text for details).

gas-phase infrared multiple photon dissociation spectroscopy (IRMPD), and density functional theory (DFT) calculations to allow a full description of the reaction mechanism, energetics, and key points governing the organocatalysts activity, including a description by the natural bond orbital (NBO) analysis of the non-covalent framework involved in the active catalyst obtained.

2. Results and Discussion

2.1. Effects of the Catalysts Structure on the Reaction Outcome

Building upon the work of Yeung et al., who employed *Cinchona*-derived organocatalysts for electrophilic bromolactonization and bromolactamization reactions in CHCl₃/PhMe mixtures, [17,61,62,66-69] we evaluated eight organocatalysts (**3a-h**) (Table 1) for the enantioselective bromoaminocyclization of *O*-cinnamyl carbamate **1** as a model reaction and to gather mechanistical insights on the reaction.

The reaction of *O*-cinnamyl carbamate 1 with 1.2 equiv of NBS was initially tested with organocatalysts 3a–g under 0.1 equiv. of catalyst loading in CHCl₃/PhMe (2:1) at -50 °C with 0.03 M of substrate concentration by 24 h (Table 1, entries 1–7). Initial evaluations of eight thiocarbamate organocatalysts (3a–g) confirmed their efficiency in catalyzing heterocycle 2 formation. The catalytic activity of cinchonine-derived catalysts 3a, 3b and 3c (Table 1, entries 1, 2, and 3 respectively) does not present sig-

nificant changes, indicating that the opposite electronic effect of the -OMe and $-CF_3$ substituents in the aryl group does not influence the stereochemical outcome.

According to Table 1, entry 4, the organocatalyst **3d** was the least active for the formation of bromoaminocyclization heterocycle **2** in 78% yield. Apparently, steric effects on substituents in the *ortho* position of the thiocarbamate group could inhibit electrophilic bromine transfer.

Two additional thiocarbamate organocatalysts were evaluated, derived from quinidine (3e) and cinchonidine (3f) (Table 1, entries 5 and 6, respectively), along with the thiourea-type organocatalyst 3g (Table 1, entry 7), also derived from cinchonidine. Despite their high efficiency in promoting the formation of compound 2, organocatalysts 3e, 3f, and 3g were not active in the formation of heterocycle 2 with appreciable levels of enantioselectivity. However, the trend observed in the enantiomeric ratios across entries 1–7 (Table 1) indicates that these pseudoenantiomeric organocatalysts, 3e and 3f, induce opposite enantiomeric preferences in the formation of product 2 (53:47 and 48:52, respectively). Even though these enantiomeric ratios indicate that 2 is formed in an almost racemic form, these results suggest that the organocatalysts exert control in the enantiomeric excess of the reaction.

A thiourea-type organocatalyst **3g** derived from cinchonidine was also tested but was also not active in the formation of heterocycle **2** at appreciable levels of enantioselectivity.

It should be noted that the reaction solvent was also evaluated at this stage to verify its influence on the enantioselectivity

Table 1. Bromoaminocyclization of 1 using catalysts with selected Cinchona chiral frameworks.a

Entry	Cat	Solvent ^{b)}	Yield [%] ^{c)}	er ^{d)}
1	3a	CHCl ₃ /PhMe (2:1)	100	57:43
2	3b	CHCl ₃ /PhMe (2:1)	100	53:47
3	3с	CHCl ₃ /PhMe (2:1)	100	57:43
4	3d	CHCl ₃ /PhMe (2:1)	78	54:46
5	3e	CHCl ₃ /PhMe (2:1)	100	53:47
6	3f	CHCl ₃ /PhMe (2:1)	100	48:52
7	3g	CHCl ₃ /PhMe (2:1)	100	45:55
8	3a	CHCl ₃ /PhMe (1:1) ^{e)}	100	69:31
9	3a	CHCl ₃ /PhMe (1:1)	100	70:30
10	3h	CHCl ₃ /PhMe (1:1)	100(69) ^{f)}	80:20

a) Reactions were carried out with 1 (0.20 mmol), catalyst (0.02 mmol) and NBS (0.24 mmol) in solvent (0.03 M) by 24 h.

levels obtained to this point (er 57:43, Table 1, entry 1 for 3a). The detailed results on the 13 different solvents tested using organocatalyst 3a are shown in Table S1. This evaluation showed that the optimal reaction condition was achieved with a mixture of chloroform and toluene in a 1:1 ratio (Table 1, entry 9), at a concentration of 0.03 M relative to O-allyl carbamate 1. In this concentration, heterocycle 2 was obtained with an enantiomeric ratio of 70:30 and yield of 100% (Table 1, entry 9).

Considering the possible concurrent reactions involving halonium ion transfer via olefin-to-olefin between the vinyl portion of organocatalysts 3a-g and the alkene group of substrate 1, [23,70] we decided to verify if inhibiting this phenomenon may enhance the efficiency of the organocatalysts. To that end, organocatalyst 3h, whose vinyl portion is saturated, was used. This organocatalyst improved the enantiomeric ratio of compound 2 to an er of 80:20, with an isolated yield of 69% (Table 1, entry 10). The absolute configuration of the major enantiomer of heterocycle 2 was assigned as (S,S) based on a comparison of its optical activity data and chiral HPLC traces with those reported by Shi et al.[50] Through this synthetic investigation, we identified a catalytic system exhibiting enantioselectivity sufficient to demonstrate the potential of organocatalyst 3h in the aforementioned title reaction. This finding has enabled a mechanistic investigation of the reaction, which is presented in this paper.

2.2. Analysis of Reaction Intermediates by ESI(+)-MS and IRMPD Spectroscopy

The species formed during the reaction were evaluated by sampling the reaction media after 10 h of reaction and analyzing this sample by ESI(+)-MS after dilution in acetonitrile (ACN), so the initial NBS concentration would be diluted to a 10⁻⁵ mol L⁻¹

Because the reaction kinetics and relative stability of the species present in the reaction media affect the intermediates and other species that could be detected in solution, [71] the use of different catalysts can allow the detection of ions representing different reaction steps. For this reason, the reaction mechanism reported is discussed based on a compilation of correlated ions observed for the catalysts 3f and 3g, as no relevant intermediate species were observed when using other catalysts. Scheme 3 shows a catalytic cycle proposed based on the m/z ratios detected by ESI(+)-MS (Figures S1 and S2) and IRMPD spectroscopy results that will be discussed in the next sections.

Besides the ions with m/z ratios assigned to the protonated catalysts ([3f + H] $^+$ and [3g + H] $^+$), protonated substrate 1 $([1 + H]^+)$ and product 2 $([2 + H]^+)$, two ions with m/z 507– 509 and 976-978 were observed, consistent with the formation of brominated intermediates. It was not possible to observe ions related to NBS or succinimide as the detection efficiency of these species was verified to be extremely low in comparison with the other species evaluated. No ions with m/z correlated to the trilateral complex mechanism, intermediate T (Scheme 2), were detected.

As described previously, the proposition of reaction mechanism solely by the evaluation of m/z values may prevent the nature of the ion to be determined, even when tandem MS is used. [72,73] In this specific case, the ions with m/z 507–509, intermediate A $[3g + Br]^+$ may show diverse Br^+ insertion sites (AI, All, and AllI-Scheme 2), and the ions with m/z 976-978 can be associated with diverse isomeric intermediates like $[3f + Br + 1]^+$ $[3f + Br + 1']^+$, where the 1' represents the enolic form of the substrate-and $[3f + H + 2]^+$.

IRMPD spectroscopy is based on the evaluation of an ion fragmentation efficiency as a function of the IR wavelength that promotes ion photodissociation. Therefore, the measured fragmentation efficiency can reveal the absorption bands of isolated ions, allowing for isomers differentiation and the determination of the nature of the species probed. [74-77]

b) The CHCl₃ used contains 1.0% v/v EtOH additive.

c) 1H NMR yield.

d) The enantiomeric ratio (er) values were determined by HPLC analysis using a Chiralpack AD-H column.

Performed at 0.1 M.

f) Isolated yield.

nbaded from https://chemistry-europe.onlinelibrary.wiley.com/doi/10.1002/cctc.202402004 by Univ of Sao Paulo - Brazil, Wiley Online Library on [05.052025]. See the Terms and Conditions (https://onlinelibrary.wiley.com/erms

-and-conditions) on Wiley Online Library for rules of use; OA articles are governed by the applicable Creative Commons

Scheme 3. Overall catalytic cycle proposal for NBS and *O*-allyl carbamate 1 reaction based on the combined ESI(+)–MS and IRMPD spectroscopy results for catalysts 3f and 3g. See Figure 2 for the complete reaction mechanism.

Therefore, the ions with m/z 507–509, and 976–978 observed were further subjected to analysis by IRMPD spectroscopy to confirm their nature, as will be discussed in detail in the next sections.

2.3. Catalyst Activation and Bromide Binding Site

Figure 1a shows the IRMPD spectrum of the intermediate with m/z 507–509 assigned as $[3g + Br]^+$ formed upon transfer of Br from NBS to the catalyst while Figure 1b,c depicts the theoretical spectra for putative structures of distinct intermediates with bromine insertion on different sites: the thiocarbamate nitrogen (AI), the thiocarbonyl sulfur atom (AII), and the quinuclidinic nitrogen (AIII) (Scheme 2).

Figure 1a shows two major bands at 3433 and 3362 cm⁻¹, assigned to the NH stretches of the secondary amines of the thiourea portion according to the theoretical spectrum of the bromine atom binding to the sulfur atom–intermediate AII (S-Br) (Figure 1b, red), which shows these NH bands at 3455 and 3362 cm⁻¹. The experimental band at 2972 cm⁻¹ was assigned to CH stretches and predicted by theoretical calculations in this same region. It is relevant to notice that the absorption bands predicted by the theoretical calculations for the Br binding on the substrate thiourea nitrogen atom (intermediate AI (N-Br) Figure 1b, blue trace) at 3268 and 3468 cm⁻¹ or the coordination on the quinuclidinic nitrogen (AIII) based on the Whitehead proposal for chlorine association at 3380 cm⁻¹ (Figure 1c, green trace) did not show similarity with the experimental spectrum.

These results show that the thiocarbonyl sulfur atom as the bromine binding site (Figure 1b) and that the Br coordination at

the other N centers can be disregarded. This evidence is in line with the experimental observation that the conversion yield is higher for thioureas and thiocarbamates than for their oxygen substituted counterparts.

It is also worth noticing that intermediate T for the trilateral complex mechanism would not be greatly influenced by this effect, as the NBS interaction in this intermediate would not take place at the (thio)carbonyl group, being an additional indirect evidence for disregarding this trilateral complex reaction pathway.

2.4. The Nature of the Enantioselective Intermediates

Figure 1d shows the IRMPD spectrum of the ion with m/z 976–978, which could be correlated to the isomeric intermediates $[3f + Br + 1]^+/[3f + Br + 1']^+$ and $[3f + H + 2]^+$, named $B_{\text{keto}}/B_{\text{enol}}$ and E, respectively.

There are four distinctive bands in this IRMPD spectrum at 2955, 3100, 3429, and 3530 cm $^{-1}$. The sharp band at 3429 cm $^{-1}$ was assigned to the catalyst thiourea N-H oscillator as it appears in the same region as the band observed for the thiourea N-H band of the isolated [3f + H] $^+$ (Figure 1d, dashed purple trace). This suggests that the thiourea N-H is not directly involved in H-bonding interactions in these intermediates as this band is not disturbed in the intermediate compared to the catalyst.

The two broader bands at 3100 and 3530 cm⁻¹ reveal relevant information on the nature of the ions with m/z 976–978. Based on the pKa value of carbamate 1 (\approx 3.7), [78,79] the *N*-tosyl-carbamate 1 can undergo tautomerization to form

vnbaded from https://chemistry-europe.onlinelibrary.wiley.com/doi/10.1002/cctc.202402004 by Univ of Sao Paulo - Brazil, Wiley Online Library on [05/05/2025]. See the Terms and Conditions (https://onlinelibrary.wiley.com/ems

-and-conditions) on Wiley Online Library for rules of use; OA articles are governed by the applicable Creative Commons

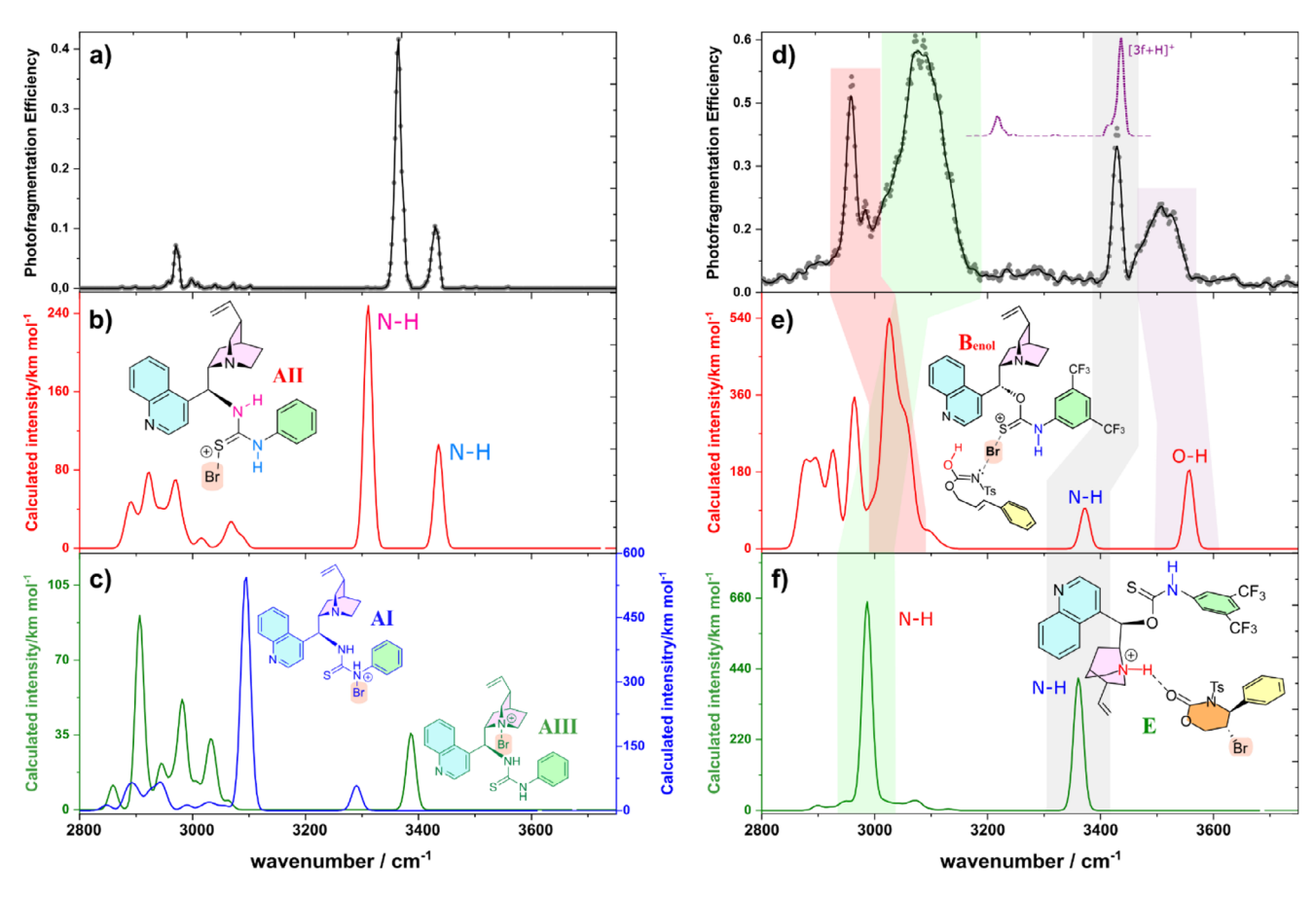


Figure 1. (a) IRMPD spectrum of intermediate m/z 507–509 observed in the reaction media of NBS, substrate 1, and catalyst 3g. Absorption spectra calculated at the B3LYP/6–311 + G(d,p) for intermediate $[3g + Br]^+$ for different bromine insertion sites: (b) sulfur atom All, (c) aryl nitrogen All (blue trace), and quinuclidinic nitrogen AllI (green trace). (d) IRMPD spectrum of intermediate m/z 976–978 observed in the reaction media of NBS, substrate 1, and catalyst 3f (black trace). Dashed purple insert shows selected experimental bands of protonated catalyst $[3f + H]^+$ for comparison. The complete IRMPD spectra of this species can be found in Figure S3. Absorption spectra calculated at the B3LYP/6–311 + G(d,p) for (e) intermediate $[3f + Br + 1']^+$ (B_{enol}-red trace) and (f) intermediate $[3f + H + 2]^+$ (E-green trace). For computational details, see Supporting Information.

N-tosyl-carbonimidate 1', and the broader band at 3530 cm⁻¹ can be assigned to a redshifted H-bonded OH stretches of 1'.

The IRMPD spectra of the substrate sodium adduct $[1 + Na]^+$ (Figure S3a) showed an NH stretch expected to be present for the keto form at 3412 cm⁻¹, in agreement with the calculations. No enolic O—H bands were observed at 3601 cm⁻¹ as predicted by the calculation, and the band at 3530 cm⁻¹ observed for the ion with m/z 976-978 suggests the enol form is only stabilized when interacting with the activated catalysts. This is in line with the fact that the enol formation would leave the nitrogen center free to interact with the Br atom (Figure 1e).

The simulated spectra of intermediate \mathbf{B}_{enol} , considering the $3\mathbf{f}$ interaction with the enolic form of the substrate and the Br insertion in the sulfur atom are shown in Figure 1e. This calculated spectrum shows two bands at 3390 and 3440 cm $^{-1}$ correlated to the thiourea N-H stretch and the H-bonded enol OH. This intermediate also shows a series of C-H oscillators assigned as those giving rise to the sharp band at 2955 cm $^{-1}$ in the experimental IRMPD spectrum.

The broad band at 3100 cm⁻¹, nevertheless, is not predicted by this calculation but was assigned to an H-bonded NH stretch of the quinuclidinic N interacting with product 2 carbonyl group ([3f + H + 2] $^+$, Scheme 3–E). This band would appear redshifted from the expected free quinuclidinic N $^+$ —H stretch of the protonated catalyst [3f + H] $^+$ observed experimentally at 3216 cm $^{-1}$ (Figure 1d, dashed purple trace).

This led us to propose that upon cyclization of the substrate from intermediate \mathbf{B}_{enol} to \mathbf{E} , the H-bonded enol gives rise to a carbonyl group, and the hydrogen atom is formally transferred to protonate the quinuclidinic N as depicted in intermediate \mathbf{E} (Figure 1f). Therefore, the protonated quinuclidinic N—H would still partially share the proton with the carbonyl oxygen, redshifting and broadening this oscillator absorption to the 3100 cm⁻¹ range observed as a broad band in the experiment, but blueshifted from the theoretical predicted formal protonated quinuclidinic N—H stretch at 2900 cm⁻¹ (Figure 1f).

These experimental and theoretical results suggest that the ion with m/z 976–978 observed could be assigned to a mixture of intermediates \mathbf{B}_{enol} and \mathbf{E} .

2.5. Origins of the Enantiomeric Control

Considering the experimental evidence discussed in the previous sections, especially the mass spectrometry results for the

vinloaded from https://chemistry-europe.onlinelbrary.wiley.com/doi/10.1002/cctc.202402004 by Univ of Sao Paulo - Brazil, Wiley Online Library on [05/05/2025], See the Terms and Conditions (https://onlinelibrary.wiley.com/terms-and-conditions) on Wiley Online Library for rules of use; OA articles are governed by the applicable Creative Commons Licenses

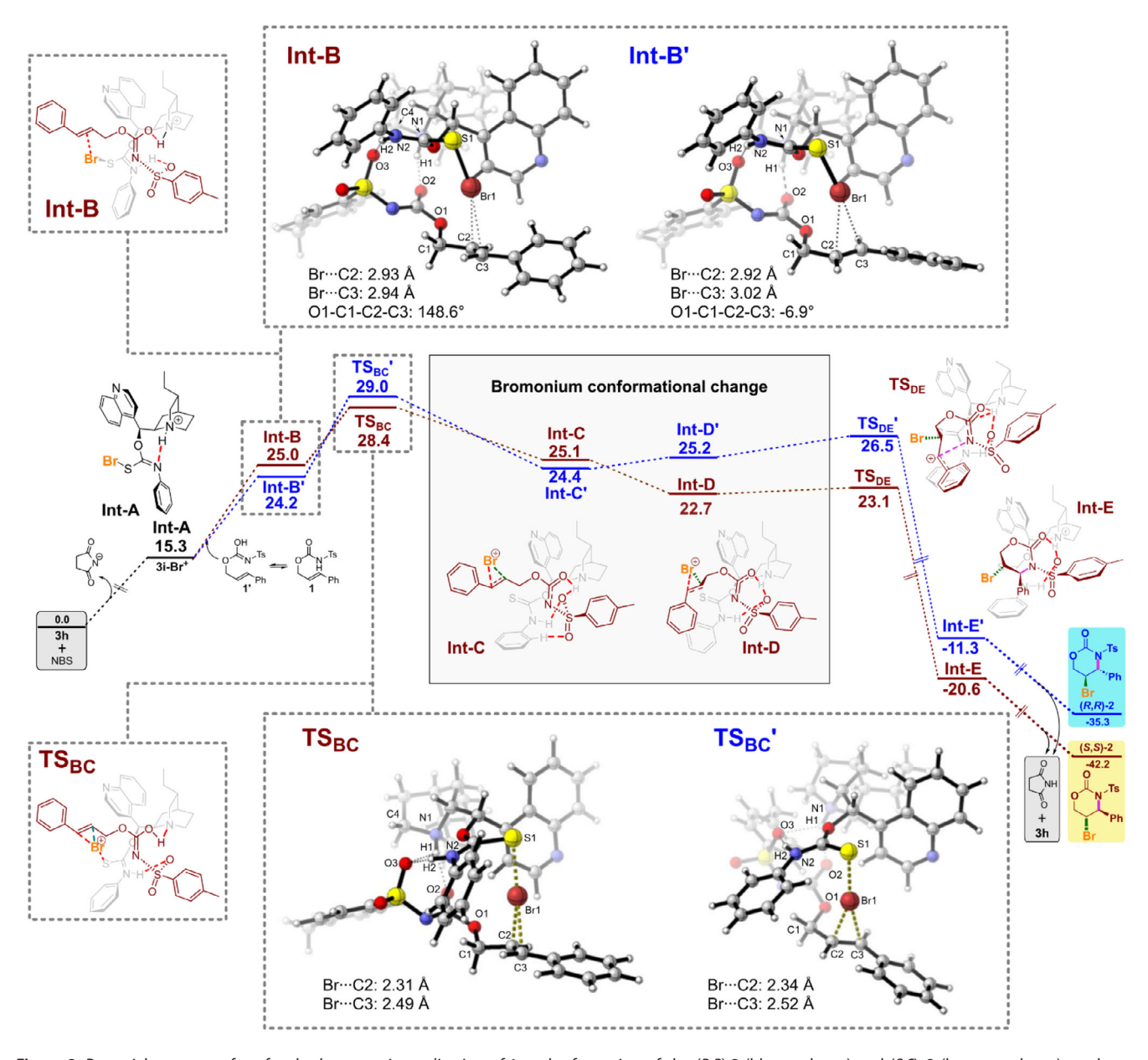


Figure 2. Potential energy surface for the bromoaminocyclization of 1 to the formation of the (R,R)-2 (blue pathway) and (S,S)-2 (brown pathway) products, calculated at the M06-2X/6-311++G(2d,2p)//M06-2X/6-31G(d,p) level of theory in CHCl₃ (SMD model) at 223.15 K. Gibbs free energy values are shown in kcal mol⁻¹. The sum of the energies of 1, NBS, and 3h are set to zero. Simplified representations of the species are shown for the (S,S)-2 products formation for simplicity. A version of this figure with the structural representation of all species can be found in Supporting Information.

reactions carried out for the organocatalysts **3f** and **3g**, the overall reaction mechanism depicted in Scheme 3 was proposed.

The reaction mechanism would start with the Br transfer from NBS to the thiourea/thiocarbamate sulfur atom, forming the active catalyst represented by All in Scheme 3. This intermediate would bind to the enol form of the substrate (1'), forming the intermediate B_{enol} that would proceed to the formation of the product-organocatalyst complex E followed by the release of the product 2, and regeneration of the catalyst. Considering the structures of the intermediates observed in this study, the transformation from B_{enol} to E was proposed to take place via a bromonium transition state.

Based on this proposal, the potential energy surface (PES) for this reaction was carried out for the most successful catalyst $\bf 3\ h$

prepared (Table 1, entry 11) using density functional theory (DFT) calculations at the M06-2X/6–311++G(2d,2p)//M06-2X/6–31G(d,p) level of theory at 223.15 K considering CHCl $_3$ as the solvation medium using the SMD model (Figure 2).[80]

The initial mechanistic step representing the Br transfer from NBS to the sulfur atom of the thiourea group followed by the transfer of a hydrogen atom of the thiourea group to the quinuclidine nitrogen a first intermediate IntA (Figure 2) compatible with the experimental results discussed in the previous sections.

Then, species 1' bind to 3h-Br $^+$ through two diverse conformations, leading to the formation of intermediates Int-B and Int-B' with relative free energies of 25.0 and 24.2 kcal mol $^{-1}$ representing the pathway that leads to the (S,S)-2 and (R,R)-2 products, respectively.

The formation of C—Br and C—N bonds occurs through stepwise mechanisms, involving two distinct transition states for each type of bond for both enantiomers. Bromine insertion proceeds via the formation of bromonium intermediates, Int-C (25.1 kcal mol^{-1}) and Int-C' (24.4 kcal mol^{-1}). The formation of Int-C' through the TS_{BC} ' transition state is responsible for the formation of the minor enantiomer (R,R)-2 is the energetically less favorable step at 29.0 kcal mol^{-1} . This step is crucial, as it dictates both the rate and stereoselectivity of the reaction mechanism. Concurrently, the formation of the bromonium ion Int-C proceeds through the transition state TS_{BC} (28.4 kcal mol⁻¹). Despite the inherent precision of the level of theory used, this transition state is 0.6 kcal mol⁻¹ more stable than TS_{BC}', leading to the formation of the major enantiomer (S,S)-2, which is in qualitative agreement with the experimentally observed enantiomeric ratio 80:20, suggesting the role of this step as the enantioselective step.

Both bromonium intermediates Int-C and Int-C' undergo conformational changes to yield Int-D (22.7 kcal mol⁻¹) and Int-D' (25.2 kcal mol⁻¹), respectively. Int-D and Int-D' intermediates form incipient secondary carbocations that may be stabilized by the conjugated π -aromatic system and aromatic stacking interactions.[81] This conformational change is essential for the carbamate group's nitrogen atom to achieve the appropriate geometry for intramolecular C-N bond formation, leading to the generation of intermediates Int-E (-20.6 kcal mol⁻¹) and Int-E' $(-11.3 \text{ kcal mol}^{-1})$, based on the $[3f + H + 2]^+$ ions (Scheme 3–E). The formation of Int-E and Int-E' proceeds through transition states TS_{DE} (23.1 kcal mol⁻¹) and TS_{DE} (26.5 kcal mol⁻¹), respectively. In the final mechanistic step, deprotonation of the organocatalyst by the succinimide anion leads to dissociation of the heterocyclic product. This yields both the major enantiomer (S,S)-2 and the minor enantiomer (R,R)-2 exergonically in -42.2 and -35.3 kcal mol⁻¹, respectively. This result indicates that the products do not deactivate the organocatalyst, regenerating it to initiate another catalytic cycle. In this way, our DFT study provides an energetically feasible mechanism that corroborates with the mass spectrometry results for the formation of both diastereomers of 2 obtained experimentally.

2.6. Non-Covalent Framework Controlling Catalytic Activity

From the experimental and theoretical evidence gathered, it is possible to consider the actual bromonium formation transition states (TS_{BC} and TS_{BC}) control the reaction enantioselectivity. These transition states (Figure 2, bottom) exhibit high structural similarity reflecting the analogous structures of their respective precursors, intermediates Int-B and Int-B' (Figure 2, top). Therefore, these species can be considered the key structures in the mechanism pathway responsible for the observed enantiodivergence.

Int-B and **Int-B**' exhibit distinct conformations of their cinnamyl moieties within the carbamate 1' partner structures. In the **Int-B** intermediate, oxygen O1 and carbon C3 adopt a *quasi-antiperiplanar* geometry with a torsional angle of 148.6°.

Consequently, the S-Br bromine atom interacts with the Si-face of carbon C2 at a distance of 2.93 Å (Figure 2, top).

In the Int-B' intermediate, due to the *synperiplanar* conformation adopted by oxygen O1 and carbon C3 (torsional angle -6.9°), the bromine atom interacts with the *Re*-face of carbon C2 at a distance of 2.92 Å.

The NBO analysis (Table S2) revealed that these intermediate interactions are controlled mainly by the interactions of the enol hydrogen of substrate 1' (H1) with the quinuclidinic nitrogen (N1) and the enolate oxygen (O2) where the proton can be considered to be shared between these groups (N1–H1⁺–O2, Table S2, entries 1Int and 2Int–the interactions discussed in this section are represented in Figure 2).

For TS_{BC}/TS_{BC} , H1 is fully transferred to N1 and the interaction of the enolate oxygen is via the protonated quinuclidinic nitrogen N1 (N1-H1⁺–O2, Table S2, entry 3TS), as depicted at the IRMPD spectrum of intermediate **E** in Figure 1d.

The interaction of Br1 and the olefin C2-C3 bond is also depicted for Int-B/Int-B' (Table S2, entry 3 Int). representing approximation of these centers before the bromonium formation. Conversely, Br1 is shown to interact directly with atoms C2 and C3 for TS_{BC} and TS_{BC} with a second order stabilization energy (E(2)) of -69.82/-64.06, and -26.67/-23.13 kcal mol $^{-1}$ for TS_{BC} / TS_{BC} , respectively (Table S2, entries 1TS and 2TS). This difference in E(2) between the interaction of Br1–C2 and Br1–C3 can be correlated to the preferential formation of 6-membered rings observed in these reactions, as the attack on the C2 that would yield the 5-membered ring is not favorable due to the greater interaction of this reactive center with the Br, leaving C3 prone for the attack.

Furthermore, it should be noted that there is also an interaction between substrate to sylate oxygen O3 and N2-H2 bond of the catalyst thiourea for both the Int-B/Int-B' and TS_{BC}/TS_{BC} (Table S2, entries 5Int and 5TS) besides a minor contribution of the interaction of the oxygen O3 to the quinuclidinic nitrogen H1 (Table S2, entries 4Int and 4TS).

This O3–H2-N2 interaction may explain why thiocarbamate derivatives of these organocatalysts do not present higher efficiency levels in this reaction as the NH is relevant in the non-covalent network, in agreement to low activity observed for the *ortho*-substituted organocatalyst **3d** (Table 1, entry 4) as the steric effect would prevent this interaction from taking place.

3. Conclusions

This work has established a model reaction to investigate the non-covalent activation of (thio)urea-based organocatalysts in the bromoaminocyclization reaction of *O*-cinnamyl tosylcarbamate 1. Our study demonstrates the suitability of thiourea-anchored *chinchona* alkaloids for this transformation, achieving an er of 80:20 and 69% yield in the synthesis of heterocycle 2. The experimental results observed for the series of catalysts presented also provided valuable mechanistic insights.

ESI(+)-MS and IRMPD spectroscopy data allowed the proposition of a catalytic cycle, showing that the reaction starts with

conditions) on Wiley Online Library for rules of use; OA articles are governed by the applicable Creative Commons

European Chemical Societies Publishing

the transfer of the NBS bromide atom to the sulfur atom of the catalyst thiourea. This intermediate reacts with the substrate. promoting its keto-enol tautomerism leading to a bromonium intermediate. No evidence for the trilateral complex involving NBS, the organocatalyst thiocarbamate and the substrate 1 in the same intermediate were observed.

DFT calculations further supported the proposed mechanism, identifying specific intermediates in the enantioselective bromoaminocyclization of O-cinnamyl carbamate (1) catalyzed by 3h. The key intermediates responsible for enantioinduction were identified as Int-B and Int-B', arising from the binding of the N-tosyl-carbonimidate tautomer (1') to the 3h-Br⁺ intermediate. These intermediates differ in the cinnamyl moiety conformation, leading to distinct transition states (TS_{BC} and TS_{BC}') for bromonium ion formation. The slightly lower energy of **TS**_{BC} compared to **TS**_{BC}' ($\Delta \Delta G^{\ddagger} = 0.6 \text{ kcal mol}^{-1}$) agrees with the preferential formation of the major enantiomer (S,S)-2. This computational study aligns well with the observed enantioselectivity and mass spectrometry data, offering a detailed mechanistic understanding for this model reaction at the molecular level.

The governing interactions on the transition state for the bromonium formation (TS_{BC}) show relevant hydrogen bonds between the tosylate group and the carbamate carbonyl group with the protonated quinuclidinic nitrogen atom and between the tosylate group and the thiourea NH group, besides the interaction of the olefin with the bromine atom. These interactions are ultimately responsible for the stabilization of the active catalytic structure involved in this reaction and the observed enantiodivergence.

This work not only offers valuable insights into the reaction pathway but also lays the foundation for the rational design of more efficient (thio)urea-based catalysts for asymmetric bromoaminocyclization reactions.

Supporting Information

Experimental and theoretical methodologies are detailed in the Supporting Information besides the synthesis of the reported species, additional reaction optimization essays, ESI(+)-MS data of the reaction mixture, IRMPD data not shown on the main text, the complete PES for both reaction pathways, the NBO results discussed in the text and the atomic coordinates and 3D rendering of all the geometrical structures of the species presented in this work. The authors have also cited additional references within the Supporting Information.[82-101]

Acknowledgements

The authors would like to acknowledge FAPESP (Grants 2014/15962-5, 2015/08539-1, 2016/21676-0, 2019/25634-9, 2021/06726-0, 2022/00498-8), CAPES (Finance code 001 and grant 23038.006960/2014-65) for substantial support for the current research. The National Laboratory for Scientific Computing (LNCC/MCTI, Brazil) is also acknowledged for providing HPC resources of the SDumont supercomputer (https://sdumont.lncc.br/). We also thank the Central Instrument Facility of UNIFESP (CEMUD), the Institute of Chemistry and its Analytical Center (Code CAIQUSP/100). Jullyane Emi Matsushima would like to thank CAPES (Grant 001) for the scholarships, Francisco Wanderson Moreira Ribeiro and Guilherme Obeid would like to thank FAPESP for the fellowships (2017/18485-1, 2023/01180-4 and 2020/08894-4) and Thiago Carita Correra would like to thank CNPg for the fellowship (306701/2023-5).

The Article Processing Charge for the publication of this research was funded by the Coordenação de Aperfeiçoamento de Pessoal de Nível Superior - Brasil (CAPES) (ROR identifier: 00×0ma614).

Conflict of Interests

The authors declare no conflict of interest.

Data Availability Statement

The data that support the findings of this study are available from the corresponding author upon reasonable request.

Keywords: Asymmetric catalysis • Cyclization • Non-covalent interactions · Organocatalysis · Reaction mechanisms

- S. Ranganathan, K. M. Muraleedharan, N. K. Vaish, N. Jayaraman, Tetrahedron 2004, 60, 5273-5308.
- [2] F. da Silva, J. Junior, M. de Mattos, Curr. Org. Synth. 2005, 2, 393-414.
- [3] A. N. French, S. Bissmire, T. Wirth, Chem. Soc. Rev. 2004, 33, 354-362.
- O. Kitagawa, T. Taguchi, Synlett 1999, 1999, 1191-1199.
- [5] O. Kitagawa, T. Sato, T. Taguchi, Chem. Lett. 1991, 20, 177-180.
- [6] S. H. Kang, S. B. Lee, C. M. Park, J. Am. Chem. Soc. 2003, 125, 15748–15749.
- [7] T. A. Doroski, M. R. Cox, J. B. Morgan, Tetrahedron Lett. 2009, 50, 5162-5164
- [8] M. R. Manzoni, T. P. Zabawa, D. Kasi, S. R. Chemler, Organometallics 2004, 23, 5618-5621.
- [9] F. E. Michael, P. A. Sibbald, B. M. Cochran, Org. Lett. 2008, 10, 793-796.
- [10] G. Yin, T. Wu, G. Liu, Chem. Eur. J. 2012, 18, 451-455.
- [11] R.-L. Li, G.-Q. Liu, W. Li, Y.-M. Wang, L. Li, L. Duan, Y.-M. Li, Tetrahedron 2013, 69, 5867-5873.
- [12] A.-D. Manick, F. Berhal, G. Prestat, Synthesis 2016, 48, 3719–3729.
- [13] J. Zhang, X. Wang, Y. Liu, X. Wang, W. He, Appl. Organomet. Chem. 2017, 31. e3631.
- [14] H.-J. Jiang, K. Liu, J. Yu, L. Zhang, L.-Z. Gong, Angew. Chem., Int. Ed. 2017, 56, 11931-11935.
- [15] X. W. Liang, X. Chen, Z. Zhang, S. L. You, Chin. Chem. Lett. 2018, 29, 1212-1214.
- [16] K. D. Ashtekar, M. Vetticatt, R. Yousefi, J. E. Jackson, B. Borhan, J. Am. Chem. Soc. 2016, 138, 8114-8119.
- [17] C. K. Tan, L. Zhou, Y.-Y. Yeung, Org. Lett. 2011, 13, 2738–2741.
- [18] G. Chen, S. Ma, Angew. Chem., Int. Ed. 2010, 49, 8306–8308.
- [19] C. Tan, L. Zhou, Y.-Y. Yeung, Synlett 2011, 2011, 1335-1339.
- [20] H. Fujioka, K. Murai, Heterocycles 2013, 87, 763-805.
- [21] A. Mendoza, F. J. Fananas, F. Rodríguez, Curr. Org. Synth. 2013, 10, 384-
- [22] A. Castellanos, S. P. Fletcher, Chem. Eur. J. 2011, 17, 5766-5776.
- S. E. Denmark, W. E. Kuester, M. T. Burk, Angew. Chem., Int. Ed. 2012, 51,
- U. Hennecke, Chem. Asian J. 2012, 7, 456-465.
- [25] J. R. Wolstenhulme, V. Gouverneur, Acc. Chem. Res. 2014, 47, 3560-3570.
- [26] A. Sakakura, K. Ishihara, Chem. Rec. 2015, 15, 728-742.
- [27] C. K. Tan, W. Z. Yu, Y.-Y. Yeung, Chirality 2014, 26, 328-343.

8673899,

- [28] S. Zheng, C. M. Schienebeck, W. Zhang, H.-Y. Wang, W. Tang, Asian J. Org. Chem. 2014, 3, 366–376.
- [29] M. Khalid, S. Mohammed, Indian J. Heterocycl. Chem. 2018, 28, 507-527.
- [30] D. Böse, S. Denmark, Synlett 2018, 29, 433-439.
- [31] V. de Andrade, M. de Mattos, Synthesis 2019, 51, 1841–1870.
- [32] J. Yan, Z. Zhou, Q. He, G. Chen, H. Wei, W. Xie, Org. Chem. Front. 2022, 9, 499–516.
- [33] S. Liu, B. Q. Zhang, W. Y. Xiao, Y. L. Li, J. Deng, Adv. Synth. Catal. 2022, 364, 3974–4005.
- [34] J. M. Bauer, W. Frey, R. Peters, Chem. Eur. J. 2016, 22, 5767-5777.
- [35] A. Kondoh, Y. Kamata, M. Terada, Org. Lett. 2017, 19, 1682–1685.
- [36] O. v. Singh, H. Han, Org. Lett. 2007, 9, 4801-4804.
- [37] D. Xing, D. Yang, Org. Lett. 2010, 12, 1068-1071.
- [38] J. M. Bauer, W. Frey, R. Peters, Angew. Chem., Int. Ed. 2014, 53, 7634-7638.
- [39] C. Loro, J. Oble, F. Foschi, M. Papis, E. M. Beccalli, S. Giofrè, G. Poli, G. Broggini, Org. Chem. Front. 2022, 9, 1711–1718.
- [40] E. J. Alexanian, C. Lee, E. J. Sorensen, J. Am. Chem. Soc. 2005, 127, 7690–7691.
- [41] H. Zhu, P. Chen, G. Liu, J. Am. Chem. Soc. 2014, 136, 1766–1769.
- [42] A. Lei, X. Lu, G. Liu, Tetrahedron Lett. 2004, 45, 1785–1788.
- [43] S. Christie, A. Warrington, C. Lunniss, Synthesis 2009, 2009, 148–154.
- [44] T. Bach, B. Schlummer, K. Harms, Chem. Eur. J. 2001, 7, 2581–2594.
- [45] C.-L. Zhu, J.-S. Tian, Z.-Y. Gu, G.-W. Xing, H. Xu, Chem. Sci. 2015, 6, 3044–3050.
- [46] S.-Q. Li, P. Xiong, L. Zhu, X.-Y. Qian, H.-C. Xu, Eur. J. Org. Chem. 2016, 2016, 3449–3455.
- [47] B. P. Spadafora, F. W. Moreira Ribeiro, J. E. Matsushima, E. M. Ariga, I. Omari, P. M. A. Soares, D. de Oliveira-Silva, E. Vinhato, J. S. McIndoe, T. Carita Correra, A. Rodrigues, Org. Biomol. Chem. 2021, 19, 5595–5606.
- [48] D. Huang, X. Liu, L. Li, Y. Cai, W. Liu, Y. Shi, J. Am. Chem. Soc. 2013, 135, 8101–8104.
- [49] H. Huang, H. Pan, Y. Cai, M. Liu, H. Tian, Y. Shi, Org. Biomol. Chem. 2015, 13, 3566–3570.
- [50] H. Pan, H. Huang, W. Liu, H. Tian, Y. Shi, Org. Lett. 2016, 18, 896–899.
- [51] H. Yang, G.-T. Fan, L. Zhou, J. Chen, Adv. Synth. Catal. 2017, 359, 1295– 1300.
- [52] J. Yan, Z. Zhou, Q. He, G. Chen, H. Wei, W. Xie, Org. Chem. Front. 2022, 9, 499–516.
- [53] S. De, A. Kumar Dan, R. Sahu, D. Das, Eur. J. Org. Chem. 2022, e202200817.
- [54] R. R. Knowles, E. N. Jacobsen, Proc. Natl. Acad. Sci. USA 2010, 107, 20678– 20685.
- [55] S. E. Wheeler, T. J. Seguin, Y. Guan, A. C. Doney, Acc. Chem. Res. 2016, 49, 1061–1069.
- [56] M. Orlandi, Phys. Sci. Rev. 2020, 5, 20180090.
- [57] A. M. F. Phillips, M. H. G. Prechtl, A. J. L. Pombeiro, Catalysts 2021, 11, 569.
- [58] D. C. Whitehead, R. Yousefi, A. Jaganathan, B. Borhan, J. Am. Chem. Soc. 2010, 132, 3298–3300.
- [59] K. Murai, T. Matsushita, A. Nakamura, S. Fukushima, M. Shimura, H. Fujioka, Angew. Chem., Int. Ed. 2010, 49, 9174–9177.
- [60] W. Zhang, S. Zheng, N. Liu, J. B. Werness, I. A. Guzei, W. Tang, J. Am. Chem. Soc. 2010, 132, 3664–3665.
- [61] L. Zhou, C. K. Tan, X. Jiang, F. Chen, Y.-Y. Yeung, J. Am. Chem. Soc. 2010, 132, 15474–15476.
- [62] Y. A. Cheng, W. Z. Yu, Y. Y. Yeung, Angew. Chem., Int. Ed. 2015, 54, 12102– 12106.
- [63] D. C. Whitehead, R. Yousefi, A. Jaganathan, B. Borhan, J. Am. Chem. Soc. 2010, 132, 3298–3300.
- [64] K. D. Ashtekar, M. Vetticatt, R. Yousefi, J. E. Jackson, B. Borhan, J. Am. Chem. Soc. 2016, 138, 8114–8119.
- [65] W. Zhang, N. Liu, C. M. Schienebeck, K. Decloux, S. Zheng, J. B. Werness, W. Tang, Chem. Eur. J. 2012, 18, 7296–7305.
- [66] L. Zhou, J. Chen, C. K. Tan, Y.-Y. Yeung, J. Am. Chem. Soc. 2011, 133, 9164–9167.
- [67] J. Chen, L. Zhou, C. K. Tan, Y.-Y. Yeung, *J. Org. Chem.* **2012**, *77*, 999–1009.
- [68] C. K. Tan, C. Le, Y.-Y. Yeung, *Chem. Commun.* **2012**, *48*, 5793–5795.
- [69] X. Jiang, S. Liu, S. Yang, M. Jing, L. Xu, P. Yu, Y. Wang, Y.-Y. Yeung, Org. Lett. 2018, 20, 3259–3262.
- [70] D. W. Tay, G. Y. C. Leung, Y. Y. Yeung, Angew. Chem., Int. Ed. 2014, 53, 5161–5164.

- [71] R. Hilgers, S. Yong Teng, A. Briš, A. Y. Pereverzev, P. White, J. J. Jansen, J. Roithová, *Angew. Chem., Int. Ed.* 2022, *61*, e202205720.
- [72] T. C. Ribeiro, F. W. M. Rodrigues-Oliveira, A. F. Correra, J. Phys. Chem. A 2019, 123, 8179–8187.
- [73] A. S. Fernandes, P. Maître, T. C. Correra, J. Phys. Chem. A 2019, 123, 1022– 1029.
- [74] K. X. Vo, K. Hirata, B. Martínez-Haya, J. Oomens, S. Ishiuchi, M. Fujii, A. Zehnacker, ChemPhysChem 2024, 26, e202400880.
- [75] T. Carita Correra, A. S. Fernandes, M. Mota Reginato, L. Colucci Ducati, G. Berden, J. Oomens, Phys. Chem. Chem. Phys. 2017, 19, 24330–24340.
- [76] R. A. J. O'Hair, N. J. Rijs, Acc. Chem. Res. 2015, 48, 329-340.
- [77] J. Yang, G. L. Tripodi, M. T. G. M. Derks, M. S. Seo, Y.-M. Lee, K. W. Southwell, J. Shearer, J. Roithová, W. Nam, J. Am. Chem. Soc. 2023, 145, 26106–26121.
- [78] L. D. Taylor, R. J. MacDonald, L. E. Rubin, J. Polym. Sci. A1 1971, 9, 3059– 3061
- [79] P. Unsworth, L. Löffler, A. Noble, V. Aggarwal, Synlett 2015, 26, 1567–1572.
- [80] All calculations were carried out with Gaussian09. Refer to the SI and the references cited therein.
- [81] S. L. Cockroft, C. A. Hunter, K. R. Lawson, J. Perkins, C. J. Urch, J. Am. Chem. Soc. 2005, 127, 8594–8595.
- [82] W. L. F. Armarego, D. D. Perrin, in *Purification of Laboratory Chemicals*, Butterworth-Heinemann, Oxford 1996.
- [83] Y. A. Cheng, W. Z. Yu, Y. Y. Yeung, J. Org. Chem. 2016, 81, 545–552.
- [84] M. Agirre, S. Henrion, I. Rivilla, J. I. Miranda, F. P. Cossío, B. Carboni, J. M. Villalgordo, F. Carreaux, J. Org. Chem. 2018, 83, 14861–14881.
- [85] S. H. Bennett, J. S. Bestwick, V. P. Demertzidou, D. J. Jones, H. E. Jones, F. Richard, J. A. Homer, R. Street-Jeakings, A. F. Tiberia, A. L. Lawrence, Nat. Chem. 2024, 16, 1177–1183.
- [86] J. Martens, G. Berden, C. R. Gebhardt, J. Oomens, Rev. Sci. Instrum. 2016, 87, 103108.
- [87] L. A. Hamlow, Y. Zhu, Z. J. Devereaux, N. A. Cunningham, G. Berden, J. Oomens, M. T. Rodgers, J. Am. Soc. Mass. Spectrom. 2018, 29, 2125–2137.
- [88] T. C. Penna, G. Cervi, A. F. Rodrigues-Oliveira, B. D. Yamada, R. Z. C. Lima, J. J. Menegon, E. L. Bastos, T. C. Correra, *Rapid Commun. Mass Spectrom.* 2020, 34, e8635.
- [89] M. J. Frisch, G. W. Trucks, H. B. Schlegel, G. E. Scuseria, M. A. Robb, J. R. Cheeseman, G. Scalmani, V. Barone, G. A. Petersson, H. Nakatsuji, X. Li, M. Caricato, A. Marenich, J. Bloino, B. G. Janesko, R. Gomperts, B. Mennucci, H. P. Hratchian, J. V. Ortiz, A. F. Izmaylov, J. L. Sonnenberg, D. Williams-Young, F. Ding, F. Lipparini, F. Egidi, J. Goings, B. Peng, A. Petrone, T. Henderson, D. Ranasinghe, et al. Gaussian 09 Revision E.01, 2015.
- [90] Y. Zhao, D. G. Truhlar, Acc. Chem. Res. 2008, 41, 157-167.
- [91] R. Ditchfield, W. J. Hehre, J. A. Pople, J. Chem. Phys. 1971, 54, 724–728.
- [92] W. J. Hehre, R. Ditchfield, J. A. Pople, J. Chem. Phys. 1972, 56, 2257–2261.
- [93] M. S. Gordon, Chem. Phys. Lett. 1980, 76, 163–168.
- [94] A. V. Marenich, C. J. Cramer, D. G. Truhlar, J. Phys. Chem. B 2009, 113, 6378–6396.
- [95] T. A. Halgren, J. Comput. Chem. 1996, 17, 490-519.
- [96] A. D. Becke, J. Chem. Phys. 1993, 98, 5648-5652.
- [97] C. Lee, W. Yang, R. G. Parr, Phys. Rev. B 1988, 37, 785–789.
- [98] R. Krishnan, J. S. Binkley, R. Seeger, J. A. Pople, J. Chem. Phys. 1980, 72, 650–654.
- [99] T. Clark, J. Chandrasekhar, G. W. Spitznagel, P. V. R. Schleyer, J. Comput. Chem. 1983, 4, 294–301.
- [100] M. J. Frisch, G. W. Trucks, H. B. Schlegel, G. E. Scuseria, M. A. Robb, J. R. Cheeseman, G. Scalmani, V. Barone, B. Mennucci, G. A. Petersson, H. Nakatsuji, M. Caricato, X. Li, H. P. Hratchian, A. F. Izmaylov, J. Bloino, G. Zheng, J. L. Sonnenberg, M. Hada, M. Ehara, K. Toyota, R. Fukuda, J. Hasegawa, M. Ishida, T. Nakajima, Y. Honda, O. Kitao, H. Nakai, T. Vreven, J. A. Montgomery, et al. Gaussian 09 Revision D.01, 2013.
- [101] A. F. Rodrigues-Oliveira, F. W. M. Ribeiro, G. Cervi, T. C. Correra, ACS Omega 2018, 3, 9075–9085.

Manuscript received: December 4, 2024 Revised manuscript received: February 28, 2025 Accepted manuscript online: March 3, 2025 Version of record online: March 16, 2025